Defect states and commensurability in dual-period $Al_xGa_{1-x}As$ photonic crystal waveguides

A. D. Bristow,[1] D. M. Whittaker,[1,*] V. N. Astratov,[1,2] M. S. Skolnick,[1] A. Tahraoui,[3,4] T. F. Krauss,[3] M. Hopkinson,[4] M. P. Croucher,[1] and G. A. Gehring[1]

[1]*Department of Physics and Astronomy, University of Sheffield, Sheffield, S3 7RH, United Kingdom*

[2]*Department of Physics, University of North Carolina, Charlotte, North Carolina 28223, USA*

[3]*School of Physics and Astronomy, University of St. Andrews, St Andrews, KY16 9SS, United Kingdom*

[4]*Department of Electronic and Electrical Engineering, University of Sheffield, Sheffield, S1 3JD, United Kingdom*

(Received 6 January 2003; revised manuscript received 20 March 2003; published 7 July 2003)

$Al_xGa_{1-x}As$ waveguides with one-dimensional dual-period patterning, consisting of a short period lattice of semiconductor stripes with periodically placed defects, are investigated by surface coupling reflectivity. Defect states, characterized by flat dispersions and enhanced optical density in the defect region, are observed within an energy gap arising from the short period modulation of the structure. When the defect width is incommensurate with the short period, strong additional features due to band folding are observed. The experimental spectra and dispersions are found to be in very good agreement with the predictions of scattering-matrix calculations.

DOI: 10.1103/PhysRevB.68.033303 PACS number(s): 42.70.Qs, 42.79.Gn, 42.79.Dj

Periodically patterned dielectric materials provide a means to control the propagation and emission of light.[1,2] In particular, they may support a photonic band gap (PBG) that has generated interest for all-optical and optoelectronic applications. However, complex fabrication requirements make it difficult to obtain a full three-dimensional (3D) band gap at optical wavelengths. Photonic crystal waveguides (PCWs) can simplify processing demands by employing a slab waveguide to confine light vertically, so the patterning is required to control the light in the in-plane direction only.[3]

The functionality of the resulting photonic crystal can be increased by incorporating light control regions, such as point defects.[4] These are analogous to the electronic donor and acceptor states in semiconductor materials, which result from the introduction of defects into the crystal, for example by substitution of dissimilar atoms at lattice or interstitials sites, or by the creation of vacancies. A widely studied example of a photonic defect is in 1D microcavity structures.[5] In 2D various types of defect have been used as resonators[6,7] to form cavities with high Q and low modal volume, while line dislocations provide waveguides that can contain low radius bends.[8] More recently, waveguiding has been achieved by chains of periodically spaced point defects, which act as coupled resonators.[9]

In this Brief Report, we investigate 1D photonic crystals fabricated by etching air trenches into AlGaAs slab waveguides. The structures consist of a short-period lattice of semiconductor stripes/air trenches, period a, interrupted by periodically placed semiconductor defects, giving a supercell period a_s. Such dual-periodicity has been theoretically investigated in fibre Bragg gratings (FBG's)[10] and in AlGaAs Bragg stacks,[11] showing narrow transmission regions in the PBG. This corresponds to a defect band which has weak dispersion in k-space and enhanced localization of electromagnetic (EM) fields in real space. The longer supercell period shrinks the Brillouin zone (BZ) from $k=\pm\pi/a$ to $k=\pm\pi/a_s$, with additional folding of the bands and creation of minigaps at the new zone boundaries. However, many features of band folding due to the smaller period are retained.

The defects are formed by increasing or decreasing the semiconductor stripe width in one unit of the supercell by an amount Δw. We consider both commensurate [Fig. 1(b)] and incommensurate [Fig. 1(c)] structures, for which Δw is, or is not, an integer multiple of the fundamental period a, respectively. In an incommensurate structure, unlike the commensurate case, the regular lattice undergoes a phase shift across each defect, as can be seen by comparing Figs. 1(b) and 1(c) with Fig. 1(a). These structures should be distinguished from quasicrystals,[14] where two incommensurate periods are combined so that there is no long-term periodicity. As we displace the lattice on either side of an inserted defect our structures are always periodic, with superperiod a_s. For point defects this issue is only relevant to 1D lattices, because in periodic 2D structures such incommensurability is not possible. However, 1D line defects can be introduced into a 2D lattice in an incommensurate way, when the defect width is not a multiple of the lattice period.[12] Fractional dislocations of this sort are being investigated as waveguides and as strategies to enhance cavity Q's.[13]

The PCW's were fabricated from an asymmetric AlGaAs planar waveguide grown by molecular beam epitaxy (MBE). The structure consists of a 240 nm $Al_{0.08}Ga_{0.92}As$ waveguide core layer, clad by 800 nm $Al_{0.9}Ga_{0.1}As$ on the lower side and air on the upper side, as shown schematically in Fig. 1(d). 1D photonic lattices were deeply etched through the core into the cladding by electron beam lithography (EBL) and reactive ion etching (RIE). A set of 80 μm$\times$80 μm regions were patterned with short-period lattice $a=295$ nm, air trench width of 65 nm, and semiconductor stripe width $w=295-65=230$ nm (air fill factor of $f\approx 22\%$). The periodic defects were introduced by adding a width Δw of semiconductor to every fifth stripe of the short period ($m=5$) to give a supercell of period $a_s=ma+\Delta w$. The defect width was varied in the range $-100\leqslant\Delta w\leqslant+295$ nm. However, the results reported here focus on (1) a reference crystal without defects ($\Delta w=0$), (2) a defect width $w_d=w+\Delta w=525$ nm, i.e., $\Delta w=+295$ nm, $a_s=1770$ nm, and (3) a defect width $w_d=330$ nm, i.e., $\Delta w=+100$ nm, a_s

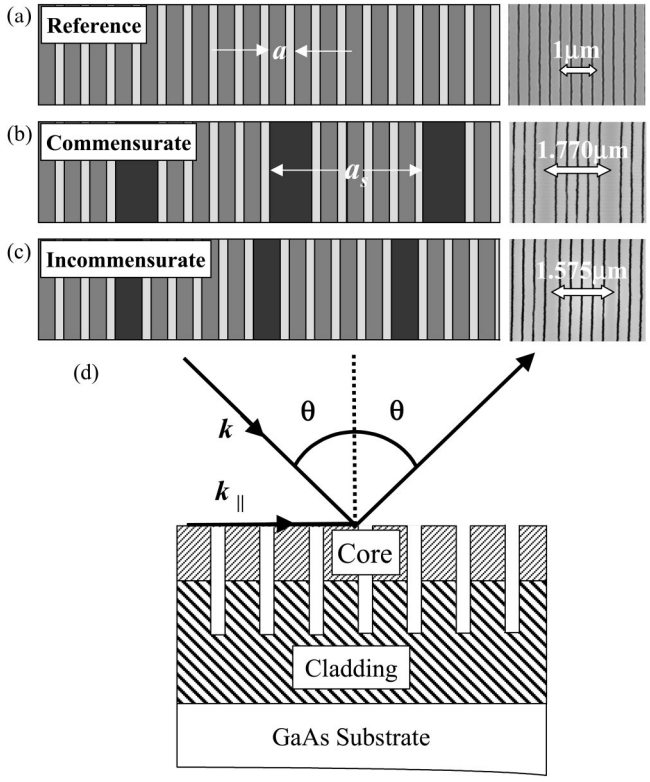

FIG. 1. Left side of (a), (b), and (c) are schematic representations of (a) the single-period reference structure, (b) the dual-period commensurate structure, and (c) the dual-period incommensurate structure. The light gray regions represent air, medium gray regions represent the semiconductor, and dark gray regions represent the semiconductor defect. a is the regular period and a_s is the supercell period. On the right-hand side, surface scanning electron micrographs of the real structures are shown. In (a) the period is $a=295$ nm, in (b) the supercell period is $a_s=1770$ nm, and in (c) $a_s=1575$ nm. (d) Schematic cross-section view of the PCW with layer structure and experimental geometry is indicated.

$=1575$ nm. Structure (3) is incommensurate, but structure (2) is commensurate since $\Delta w=a$, as can be seen by inspections of the surface scanning electron micrographs (SEM's) shown on the right hand side of Figs. 1(a)–1(c).

The structures were investigated experimentally by surface coupling reflectivity, shown in Fig. 1(d), in which external EM radiation is coupled to the leaky modes of the photonic band structure.[15–17] Measurements were performed by varying the polar angle, allowing direct determination of the dispersion of the photonic bands, since light incident at angle θ with frequency ω can couple to modes in the waveguide with wave vector $k_{\parallel}=(\omega/c)\sin\theta$, as required by in-plane wave vector conservation across the air-photonic crystal interface. This provides information about both the defect modes and the folded modes in the supercell BZ. In the commensurate structures these latter features are weak, but they are much stronger in the incommensurate case, because of the phase shifts in the lattice across the defects. For 1D PCWs, the transverse-electric (TE) and transverse-magnetic (TM) band structures are nearly identical, except for a small energy splitting, so only the measurements for TE polarized light are presented here.

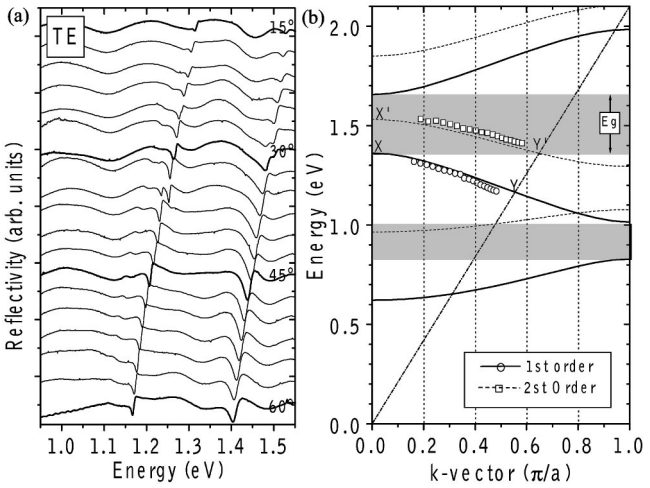

FIG. 2. (a) Experimental reflectivity spectra for the reference sample (without defects), between $15°\leqslant\theta\leqslant 60°$ in TE polarization. (b) Calculated band structure for first- and second-order confined vertical modes with the experimental points obtained from the reflectivity spectra. The gray regions indicate the first-order PBGs.

A series of reflectivity spectra for the reference structure[18] without defects is shown in Fig. 2(a) for a range of polar angles $15°\leqslant\theta\leqslant 60°$ in a plane perpendicular to the grooves of the structure. Two modes are observed moving toward decreasing energy when the angle is increased. The corresponding dispersion is plotted in Fig. 2(b). By comparing with scattering-matrix (S-matrix) calculations,[19] we find that the lower energy band is a first-order vertically confined mode and the higher energy band is a second-order mode. As in our previous work on 2D lattices the second-order mode is confined due to natural oxidation of the high Al concentration cladding region; this leads to lowering of the refractive index of the cladding, which increases confinement.[16] The gray regions indicate the PBG for TE polarized, first-order vertically confined light.

Reflectivity spectra as a function of polar angle for the incommensurate $\Delta w=+100$ nm structure are shown in Fig. 3(a), with accompanying theoretical spectra in Fig. 3(b). Many more features are now visible in the spectra than were seen for the single period sample in Fig. 2, with bands that increase, decrease, and anticross as the angle is varied. There is good agreement between the experimental and theoretical spectra. In Fig. 4(a) the dispersions are plotted in the reduced zone scheme corresponding to the supercell BZ for $a_s=1575$ nm, which is 5.3 times smaller than that of Fig. 2(b). Appropriate reciprocal lattice vectors of $2\pi/a_s$ are subtracted from the experimental k values to translate the points back into the reduced BZ.

It is clear that the new features labeled α, β, γ in Fig. 4(a) arise from zone folding of the first-order short-period bands of Fig. 2. At the BZ boundary new minigaps open up, thus accounting for the observed anticrossings. The overall extent in k space of the α, β, γ bands together is approximately equivalent to that of the unfolded band between points X and Y in Fig. 2(b) for the reference sample, from $k=0$ to the boundary of the observable region in surface reflectivity experiments defined by the light line (shown by

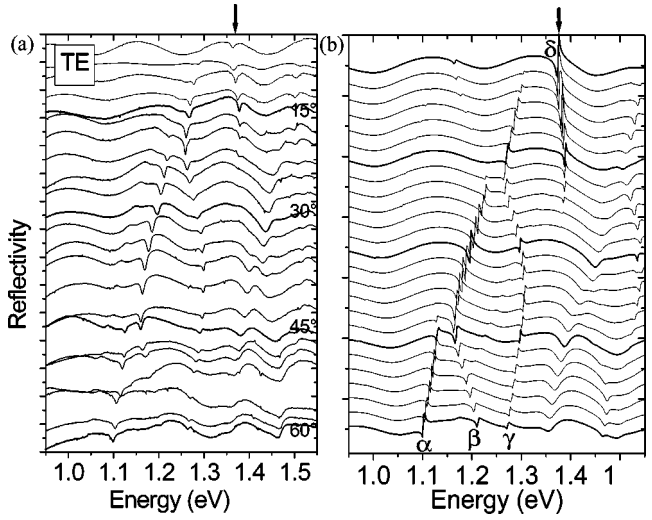

FIG. 3. (a) Experimental reflectivity spectra for the PCW sample, which has defects and dual periodicity with $\Delta w = +100$ nm ($a_s = 1575$ nm), between $5° \leqslant \theta \leqslant 60°$ in TE polarization. (b) Theoretical comparison calculated by the *S*-matrix method for angles $0° \leqslant \theta \leqslant 60°$. In both (a) and (b) the defect mode, indicated by arrows, is clearly visible at ~ 1.375 eV and has relatively flat dispersion. Band labels are assigned to aid comparison with Fig. 4.

diagonal construction line). Similar correspondence of the second-order modes (open squares) in Fig. 4(a) occurs with the regions between X' and Y' in Fig. 2. By contrast, when plotted in the BZ of the short period, as employed in Fig. 2(b), the dispersions are complicated and difficult to analyze (not shown).

In addition to the dispersive bands, a prominent nondispersive mode is observed at low angles in Fig. 3 at about ~ 1.375 eV, and is indicated by the filled circles in Fig. 4(a) (denoted δ). We attribute this feature to a defect mode lying in the first-order PBG of the regular lattice, labeled E_g and

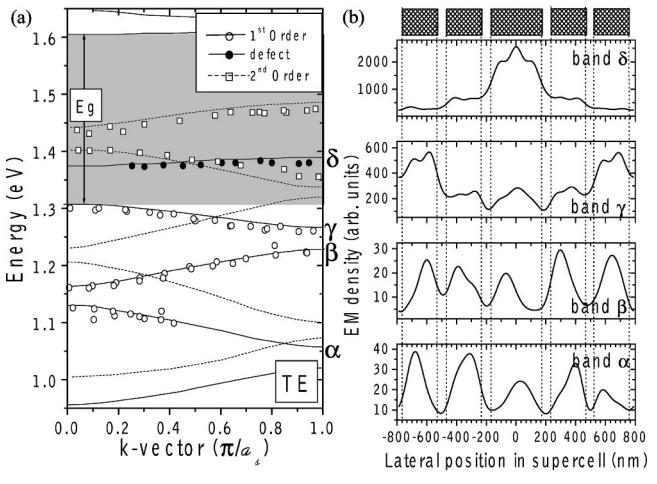

FIG. 4. (a) Theoretical bandstructure for the $\Delta w = +100$ nm sample with overlaid experimental points. Bands α through δ are labeled for comparison of their in-plane electromagnetic density shown in (b) for $k = 0.6$, chosen arbitrarily to be close to the center of the BZ.

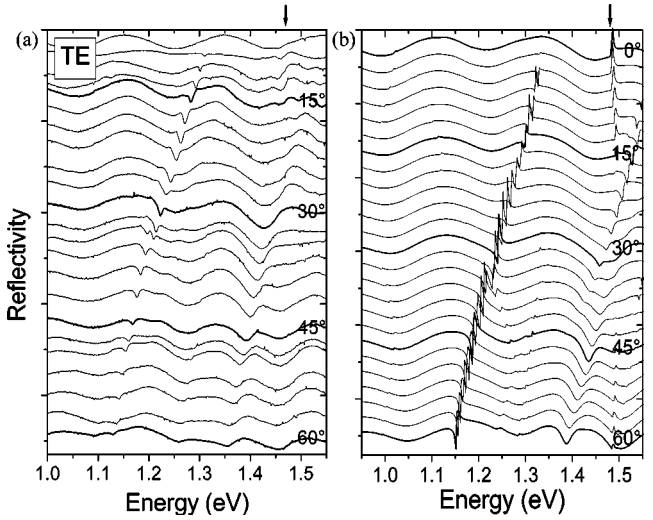

FIG. 5. (a) Experimental reflectivity spectra for the PCW sample with $\Delta w = +295$ nm ($a_s = 1770$ nm), between $5° \leqslant \theta \leqslant 60°$ in TE polarization. (b) Theoretical comparison calculated by the *S*-matrix method for angles $0° \leqslant \theta \leqslant 60°$. In both (a) and (b) the defect mode, indicated by arrows, is visible at ~ 1.48 eV and has relatively flat dispersion.

indicated by the shaded gray region [Figs. 2(b) and 4(a)]. The defect mode is not observed in the reflectivity spectra much beyond the edge of the first supercell BZ ($\approx 20°$ at this energy, giving a $\Delta k = 2.38 \times 10^8$ cm^{-1}). This visibility is determined by the extent of the mode in k space, and corresponds to the Fourier transform of the localization in real space, giving $1/\Delta k = 420$ nm, which is slightly more than one semiconductor defect stripe.

The assignment of dispersive and defect modes is confirmed by *S*-matrix calculations of the in-plane EM field densities for bands α, β, γ shown in Fig. 4(b). Band δ, also shown in Fig. 4(b), is localized within the defect region, providing strong additional evidence for its attribution to a localized defect mode. By contrast, bands α, β, γ are much more extended over the supercell, and indeed tend to be excluded from the defect region.

Experimental and theoretical analyses of several other structures in the range $-100 \leqslant \Delta w \leqslant +295$ nm were performed. Each of the incommensurate structures showed strong coupling to all dispersive and localized modes. Experimental and theoretical spectra from the commensurate $\Delta w = +295$ nm structure are shown in Fig. 5. As in Fig. 3, a good agreement between experiment and theory is found. For small angles, a nondispersive defect mode is seen at ~ 1.48 eV, lying once again in the region of the PBG of the regular period. As before, this feature becomes weak at the edge of the supercell BZ, which in this case occurs at $\approx 15°$. Unlike the $\Delta w = +100$ nm sample in Fig. 3, the only other strong features in the spectra of this commensurate structure[20] are two bands whose energy decreases with angle. These are very similar to those found in the reference sample in Fig. 2, arising from first- and second-order vertically confined modes as before. The other folded modes only appear as very weak spectral features, more clearly seen in the theoretical results.

Calculations of the $\Delta w = +295$ nm commensurate band structure show that it is similar to the incommensurate case. However, the folded bands of the commensurate structure are much weaker in reflectivity. This marked difference can be understood by considering the factors affecting the visibility of the modes in reflectivity. The strength of a coupling feature, for a particular photonic band structure mode, is determined by the small wave vector Fourier components of the Bloch function of that mode (typically only that corresponding to the lowest reciprocal lattice vector $G=0$).[16,19] If the bands for the regular lattice without defects are plotted in the superperiod BZ, the folding is not physical, so there is no mixing to introduce new small wave vector components, and only one visible band is visible for each $k_{\|}$. When defects are introduced, the dispersive bands can be considered as sections of unperturbed Bloch functions in the regions of regular lattice, modified close to the defect. For the commensurate case the regions on either side of the defect look identical to the perfect lattice, so if the defect could be ignored the visibility would be the same. In reality the defect cannot be ignored and it mixes some small wave vector components into the other folded bands, so they are observed, but only weakly. In the incommensurate case, there is an additional effect due to regions of lattice on either side of a defect being phase shifted. Then *every* reciprocal lattice vector component of the original Bloch function gains small wave vector components, proportional to $(1/G)[1-e^{(k_{\|}+G)\delta}]$, where δ is the phase shift. This enhances the coupling strength of all the folded bands, making them much more visible in reflectivity, as observed both experimentally and in the numerical simulations.

To conclude, both commensurate and incommensurate dual-period 1D photonic crystal waveguides have been studied by external reflectivity techniques. In both cases resonant coupling to a localized defect mode, which lies in the band gap of first-order vertically confined modes, is seen. For incommensurate structures strong coupling to folded modes in the reduced BZ of the long-period lattice is also observed. The zone folding features are, however, much weaker in commensurate structures when the supercell period is an integer multiple of the small period.

This work was funded by EPSRC Grant No. GR/M72951/01.

*Author to whom correspondence should be addressed. Electronic address: d.m.whittaker@sheffield.ac.uk

[1] E. Yablonovitch, Phys. Rev. Lett. **58**, 2059 (1987).
[2] S. John, Phys. Rev. Lett. **58**, 2486 (1987).
[3] T.F. Krauss, R.M. De La Rue, and S. Brand, Nature (London) **383**, 699 (1996).
[4] J.D. Joannopoulos, P.R. Villeneuve, and S. Fan, Nature (London) **386**, 143 (1997).
[5] M.S. Skolnick, T.A. Fisher, and D.M. Whittaker, Semicond. Sci. Technol. **13**, 645 (1998).
[6] O.J. Painter, A. Husain, A. Scherer, J.D. O'Brien, I. Kim, and P.D. Dapkus, J. Lightwave Technol. **17**, 2082 (1999).
[7] H. Benisty, C. Weisbuch, D. Labilloy, M. Rattier, C.J.M. Smith, T.F. Krauss, R.M. De La Rue, R. Houdré, U. Oesterle, C. Jouanin, and D. Cassagne, J. Lightwave Technol. **17**, 2063 (1999).
[8] M. Lončar, D. Nedeljković, T. Doll, J. Vučković, A. Scherer, and T.P. Pearsall, Appl. Phys. Lett. **77**, 1937 (2000).
[9] S. Olivier, C. Smith, M. Rattier, H. Benisty, C. Weisbuch, T. Krauss, R. Houdré, and U. Oesterle, Opt. Lett. **26**, 1019 (2001).
[10] R. Shimada, T. Koda, T. Ueta, and K. Ohtaka, J. Appl. Phys. **90**, 3905 (2001).
[11] S. Lan, S. Nishikawa, and O. Wada, Appl. Phys. Lett. **78**, 2101 (2001).
[12] M. Notomi, K. Yamada, A. Shinya, J. Takahashi, C. Takahashi, and I. Yokohama, Phys. Rev. Lett. **87**, 253902 (2001).
[13] T. Yoshie, J. Vučković, A. Scherer, H. Chen, and D. Deppe, Appl. Phys. Lett. **79**, 4289 (2001).
[14] L. Dal Negro, C.J. Oton, Z. Gaburro, L. Pavesi, P. Johnson, A. Lagendijk, R. Righini, M. Colocci, and D.S. Wiersma, Phys. Rev. Lett. **90**, 055501 (2003).
[15] V.N. Astratov, I.S. Culshaw, R.M. Stevenson, D.M. Whittaker, M.S. Skolnick, T.F. Krauss, and R.M. De La Rue, IEE J. Lightwave Technol. **17**, 2050 (1999).
[16] V.N. Astratov, D.M. Whittaker, I.S. Culshaw, R.M. Stevenson, M.S. Skolnick, and T.F. Krauss, R.M. De La Rue, Phys. Rev. B **60**, R16 255 (1999).
[17] A.D. Bristow, V.N. Astratov, R. Shimada, I.S. Culshaw, D.M. Whittaker, M.S. Skolnick, A. Tahraoui, and T.F. Krauss, IEEE J. Quantum Electron. **38**, 880 (2002).
[18] For further discussion of the band structure of a similar structure see Ref. 11.
[19] D.M. Whittaker and I.S. Culshaw, Phys. Rev. B **60**, 2610 (1999).
[20] Calculations for defect sizes from $\Delta w = +0$nm up to $+na$ where $n=3$ or 4 show that for all commensurate structures, the reflectivity spectra simplify; the zone folded dispersive modes are only very weakly visible and the minigaps of the incommensurate case close up.